PHOTONICS Research

Digital quantum simulation of Floquet topological phases with a solid-state quantum simulator

Bing Chen,[1,2] Shuo Li,[3] Xianfei Hou,[1] Feifei Ge,[1] Feifei Zhou,[1] Peng Qian,[1] Feng Mei,[4,5,7] Suotang Jia,[4,5] Nanyang Xu,[1,8] and Heng Shen[2,6,9]

[1]School of Electronic Science and Applied Physics, Hefei University of Technology, Hefei 230009, China
[2]State Key Laboratory of Quantum Optics and Quantum Optics Devices, Institute of Opto-Electronics, Shanxi University, Taiyuan 030006, China
[3]Stanford Institute for Materials and Energy Sciences, Menlo Park, California 94025, USA
[4]State Key Laboratory of Quantum Optics and Quantum Optics Devices, Institute of Laser Spectroscopy, Shanxi University, Taiyuan 030006, China
[5]Collaborative Innovation Center of Extreme Optics, Shanxi University, Taiyuan 030006, China
[6]Clarendon Laboratory, University of Oxford, Oxford OX1 3PU, UK
[7]e-mail: meifeng@sxu.edu.cn
[8]e-mail: nyxu@hfut.edu.cn
[9]e-mail: hengshen@nbi.dk

Received 30 July 2020; revised 15 October 2020; accepted 15 November 2020; posted 18 November 2020 (Doc. ID 404163); published 24 December 2020

Harnessing the dynamics of complex quantum systems is an area of much interest and a quantum simulator has emerged as a promising platform to probe exotic topological phases. Since the flexibility offered by various controllable quantum systems has helped gain insight into the quantum simulation of such complicated problems, an analog quantum simulator has recently shown its feasibility to tackle the problems of exploring topological phases. However, digital quantum simulation and the detection of topological phases still remain elusive. Here, we develop and experimentally realize the digital quantum simulation of topological phases with a solid-state quantum simulator at room temperature. Distinct from previous works dealing with static topological phases, the topological phases emulated here are Floquet topological phases. Furthermore, we also illustrate the procedure of digitally simulating a quantum quench and observing the nonequilibrium dynamics of Floquet topological phases. Using a quantum quench, the 0- and π-energy topological invariants are unambiguously detected through measuring time-averaged spin polarizations. We believe our experiment opens up a new avenue to digitally simulate and detect Floquet topological phases with fast-developed programmable quantum simulators.

https://doi.org/10.1364/PRJ.404163

1. INTRODUCTION

Floquet systems that are generally defined by periodically driven or time-dependent Hamiltonians with $\mathcal{H}(t+T)=\mathcal{H}(t)$ for a fixed period T offer new opportunities to observe quantum Floquet matter [1]. In the area of topology, one appealing aspect of Floquet engineering is the ability to generate Floquet topological phases of matter [2–4] that are inaccessible in static equilibrium systems, thus providing a way to better understand the associated influence such as Floquet Majorana modes [5–7], anomalous topological phases with a zero Chern number [2,3], and a chiral topological phase with 0- or π-energy topological edge states [8–10]. Searching a topological phase of matter has raised considerable attention in condensed-matter physics; however, realizing Floquet-engineered topological phases in materials remains theoretical.

Remarkable advances in quantum simulation [11,12] have revolutionized our understanding of complex systems. A high degree of controllability enables ultracold atoms [13–15], trapped ions [16,17], superconducting circuits [18,19], and photonic systems [20] to offer the feasibility to tackle problems that are intractable on classical computers. Quantum simulators would not only unveil new results that cannot be otherwise predicted or classically simulated, but they would also allow us to test various models. For instance, analog quantum simulators (AQSs) mimic the time evolution of one specific model Hamiltonian; as a result, they are used to investigate the topological phases and effects with great experimental progresses recently [21–39]. As the counterpart of AQS, digital quantum simulation (DQS) [11,12,40–43] encodes the state of the quantum system onto qubits and emulates the time evolution through repeated cycles of qubit rotations (quantum gates) by means of a quantum algorithm. Such a circuit-based simulator can, in principle, efficiently simulate any finite-dimensional local Hamiltonian, hence owning the advantage of universality.

Although the DQS of many-body physics has been intensively studied in various programmable quantum simulators [44–50], digital simulation and detection of topological phases are still less explored [51].

In this paper, we report the realization of the DQS of Floquet topological phases in a solid-state digital quantum simulator at room temperature [52,53]. In contrast to the AQS approach simulating static topological phases and anomalous π modes in a photonic system [54], it is illustrated here that digital quantum simulator constitutes a natural platform to simulate Floquet topological phases. We further exhibit the DQS of a quantum quench and observe the nonequilibrium dynamics of Floquet topological phases. Most strikingly, after such quench, we show that the signature 0- and π-energy topological invariants associated with Floquet topological phases could be detected through measuring the time-averaged spin polarizations, where the experimental observation is in good agreement with theoretical results. We also report the first experimental observation of the topological winding number $\nu = 5$, which is much higher than one. Further applications of this protocol could enable studies of high-dimensional and complex Floquet topological phases that go beyond the conventional topological systems [55,56].

2. RESULTS

Floquet topological phases. In this work, we consider simulating the two-band Floquet topological insulator phases described by this Floquet Hamiltonian,

$$H_F = d_x(k_x)\sigma_x + d_y(k_x)\sigma_y, \tag{1}$$

where d_x and d_y are the spin-orbit fields. Specifically, we simulate a one-dimensional (1D) periodically driven system formed by two units in one driven period [57,58]. Suppose U is the Floquet operator that describes such a periodically driven system evolving over one period T; i.e.,

$$\hat{U} = e^{-iH_2\frac{T}{2}}e^{-iH_1\frac{T}{2}}, \tag{2}$$

where $\hat{H}_1 = t_y \sin(k_x)\hat{\sigma}_y$ and $\hat{H}_2 = t_x \cos(k_x)\hat{\sigma}_x$. Then, the Floquet Hamiltonian H_F describing the emerged Floquet topological phases is defined as

$$\hat{U} = e^{-i\hat{H}_F T}. \tag{3}$$

As we will show, H_1 and H_2 both can be simulated by applying two microwave pulses on the solid-state NV-center qubit, which further allows us to digitally realize the Floquet operator U.

Regarding a Floquet topological system, there are two quasi-energy gaps centered around $E = 0$ and $E = \pi$. The topological features of Floquet topological phases are rooted in these gaps, which are characterized by the topological invariants ν_0 and ν_π, respectively. According to bulk-edge correspondence associated with topological phases, the values of topological invariants defined in the momentum space count the number of the edge modes defined in the real space. The edge modes correspond to the eigenmodes of the real-space lattice Hamiltonian with their densities maximally localized at the edges. In our Floquet topological systems, the value of ν_0 (ν_π) determines the number of the edge modes with eigenenergy $E = 0$ ($E = \pi$).

The topological invariants ν_0 and ν_π are defined in terms of a symmetry time framework [8], where the starting time point of the Floquet operator U is shifted to two symmetry time points, leading to the following two Floquet operators:

$$\hat{U}_1 = e^{-i\hat{H}_1\frac{T}{4}}e^{-i\hat{H}_2\frac{T}{2}}e^{-i\hat{H}_1\frac{T}{4}}, \quad \hat{U}_2 = e^{-i\hat{H}_2\frac{T}{4}}e^{-i\hat{H}_1\frac{T}{2}}e^{-i\hat{H}_2\frac{T}{4}}. \tag{4}$$

Both can be further rewritten in terms of Floquet Hamiltonian as

$$\hat{U}_1 = e^{-i\hat{H}_{F1}T}, \quad \hat{U}_2 = e^{-i\hat{H}_{F2}T}, \tag{5}$$

where $\hat{H}_{F1,F2} = E\mathbf{n}_\mathbf{s}\cdot\hat{\sigma}$, with $\mathbf{n}_\mathbf{s} = (n_{sx}, n_{sy}, 0)$ $(s = 1, 2)$ [59], $E = \pm\arccos\{\cos[t_x\cos(k_x)]\cos[t_y\sin(k_x)]\}$, and $\hat{\sigma} = (\hat{\sigma}_x, \hat{\sigma}_y, \hat{\sigma}_z)$ are Pauli spin operators.

Of great interest is the fact that both $\hat{H}_{F1}$ and $\hat{H}_{F2}$ are protected by a chiral symmetry with the chiral operator $\hat{\Gamma} = \hat{\sigma}_z$, supporting chiral topological phases characterized by these topological winding numbers,

$$\nu_s = \frac{1}{2\pi}\int \mathrm{d}k_x(n_{sx}\partial_{k_x}n_{sy} - n_{sy}\partial_{k_x}n_{sx}), \quad s = 1, 2. \tag{6}$$

The topological invariants ν_0 and ν_π are defined as

$$\nu_0 = \frac{\nu_1 + \nu_2}{2}, \quad \nu_\pi = \frac{\nu_1 - \nu_2}{2}. \tag{7}$$

Figure 1 presents the numerical results of the values of the topological invariants ν_0 and ν_π as a function of t_x and t_y. Surprisingly, such a simple periodically driven system has a rich topological phase diagram, and even can support topological phases with topological invariants larger than one [57,58]. On the other hand, a topological phase transition is known to occur accompanied by a gap closing. In Fig. 1, we also plot the quasi-energy gap closing points at $E = 0$ and $E = \pi$. It is shown that the values of the topological invariant ν_0 (ν_π) would change when crossing the gap closing at $E = 0$ ($E = \pi$).

Digital simulation of Floquet topological phases. To digitally simulate the Floquet operator $\hat{U}(T)$ (the time evolution of the Floquet topological Hamiltonian $\hat{H}_F$), we use a

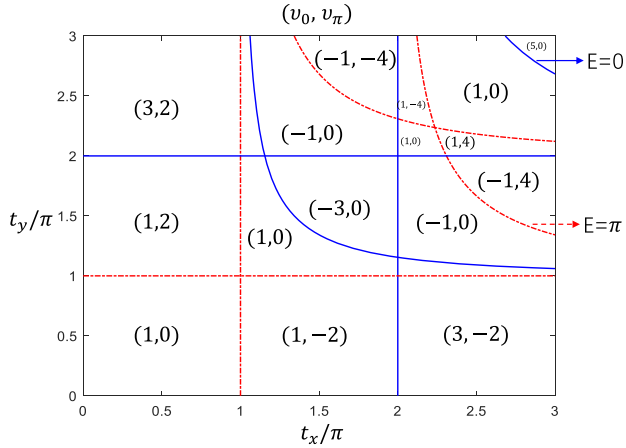

Fig. 1. Topological winding numbers (ν_0, ν_π) as a function of t_x and t_y. The red and blue solid lines separating different topological phases correspond to the gap closings at $E = 0$ and $E = \pi$, respectively.

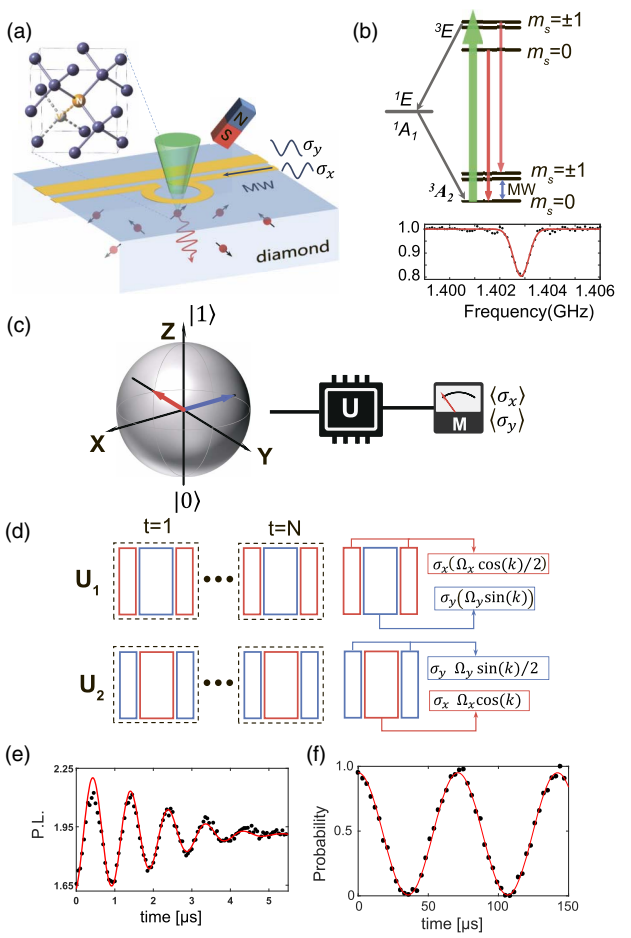

Fig. 2. (a) Illustration of experiment schematics and atomic structure of the nitrogen-vacancy (NV) center in diamond. (b) Scheme of energy levels of the NV center electron spin. Both its ground state ($^3A_2$) and excited state (^3E) are spin triplets, and the transition between the two states corresponds to the zero-phonon line (ZPL) at 637 nm (1.945 eV). The ground state ($^3A_2$) is a spin triplet with a zero-field splitting of 2.87 GHz between $m_s = 0$ and $m_s = \pm 1$ states. (c) Schematic of digital quantum simulation. The spin is prepared in the superposition state of $m_s = 0$ and $m_s = -1$. The symbol of **U** represents N series of the Floquet operators U_1 and U_2 which are shown in detail in (d). Then, we measure the time evolution of the spin polarization $\langle\hat{\sigma}_{x,y}\rangle$ represented by the meter. (e) The Ramsey oscillation of the electron spin coherence. The data were taken with the microwave detuning of 1.0 MHz by varying the temporal separation between the two microwave $p/2$ pulses. The Ramsey signal was fitted to $\exp[-(\tau/T_2^*)^2]\cos(2\pi f t)$ (blue line), where f values correspond to the microwave detuning, obtained $T_2^* = 2.59 \pm 0.14$ μs. (f) Electron-spin Rabi oscillation driven by microwave. The length of π microwave pulse is 35.0 ns by fitting the Rabi oscillation signal.

negatively charged nitrogen-vacancy (NV) center in type-IIa, single-crystal synthetic diamond sample (Element Six). $m_s = -1$ and $m_s = 0$ in $^3A_2$ are encoded as spin down $|g\rangle$ and up $|e\rangle$ of the electron spin qubit (Fig. 2). The state of the qubit can be manipulated with microwave pulses ($\omega_{MW} = 2\pi \times 1404.3$ MHz), while the spin level $m_s = +1$ remains idle due to large detuning. By applying a laser pulse of 532 nm wavelength with the assistance of intersystem crossing (ISC) transitions, the spin state can be polarized into $m_s = 0$ in the ground state. This process can be used to initialize and read out the spin state of the NV center. The fluorescence photons are detected using the single photon counting module (SPCM). By using a permanent magnet, a magnetic field (about 520 G) is applied along the NV axis, and the nearby nuclear spins are polarized by optical pumping, improving the coherence time of the electron spin.

The key ingredient in our experiment is to individually engineer the time evolution of the Hamiltonian $\hat{H}_1 = t_y \sin(k_x)\hat{\sigma}_y$ and $\hat{H}_2 = t_x \cos(k_x)\hat{\sigma}_x$, offered by such a well-controlled solid state quantum simulator [60]. Both of the Hamiltonians can be emulated by manipulating the electron spin qubit via a microwave pulse with $\hat{H}_1 = \Omega_y\hat{\sigma}_y, \hat{H}_2 = \Omega_x\hat{\sigma}_x$ and the associated Rabi frequencies Ω_x and Ω_y. Therefore, by tuning $\Omega_x = t_x \cos(k_x)$, $\Omega_y = t_y \sin(k_x)$, the Floquet operators depicted in Eq. (4) can be naturally simulated in a digital way [Figs. 2(c) and 2(d)]. It is worth mentioning that this method is genetic and not limited to the 1D topological phases studied here. This approach can be also mapped into the high-dimensional Brillouin zone and generalized to digital simulation of the Floquet operators associated with high-dimensional Floquet topological phases.

Digital simulation of quantum quenches and detection of topological invariants. The topological invariants ν_0 and ν_π featuring the topological properties of the quasi-energy gaps centered around $E = 0$ and $E = \pi$ are seminal hallmarks of Floquet topological phases [8]. Recent theoretical study has shown that, after a quantum quench, the topological invariants associated with static topological phase can be directly measured through the time-averaged spin polarizations on the band inversion surfaces (BISs) [61]. We thus proceed to show that such a method also can be used to measure the topological invariants associated with Floquet topological phases. Specifically, we digitally perform a quantum quench of Floquet topological phases and employ such a quench to measure the topological winding numbers ν_1 and ν_2, allowing us to detect the topological invariants ν_0 and ν_π according to Eq. (7).

Here is the quantum quench procedure. First, the initial state of the system is initialized in the ground state of a trivial Floquet topological Hamiltonian $\hat{H}_F^i$. Then, N series of the Floquet operators $\hat{U}_{1,2}$ are digitally performed, as shown in Fig. 2(c) or 2(d), which digitally simulates the time evolution of a nontrivial Floquet topological Hamiltonian over N periods; i.e.,

$$\hat{U}_1^N = e^{-iN\hat{H}_{F1}T}, \quad \hat{U}_2^N = e^{-iN\hat{H}_{F2}T}. \tag{8}$$

As a consequence, a sudden change from a trivial Floquet topological phase to a nontrivial Floquet topological phase is effectively performed, realizing a quantum quench. The initial quantum state will thereby evolve under the final Hamiltonian $\hat{H}_{F1,F2}$.

In our work, two cases in detail are exhibited: (1) $t_x = 0.5\pi$, $t_y = 0.5\pi$, with $(\nu_1 = 1,\ \nu_2 = 1)$ and $(\nu_0 = 1,\ \nu_\pi = 0)$; (2) $t_x = 2.5\pi$, $t_y = 0.5\pi$, with $(\nu_1 = 1,\ \nu_2 = 5)$ and $(\nu_0 = 3,\ \nu_\pi = -2)$. In particular, we implement a y-direction quench for the Floquet topological Hamiltonian $\hat{H}_{F1}$ and

an x-direction quench for the Floquet topological Hamiltonian $\hat{H}_{F2}$.

To measure the topological winding number ν_1 in case (1), the initial state of the system is prepared into $|\psi(t=0)\rangle = (|g\rangle - i|e\rangle)/\sqrt{2}$, the ground state of a trivial topological Hamiltonian $\hat{H}^i_{F1} = n_{1x}\hat{\sigma}_x + (m_y + n_{1y})\hat{\sigma}_y$ with $m_y \gg 1$. After that, we repeat $\hat{U}_1$ operation N times. Consequently, the dynamics of the initial state $|\psi(t=0)\rangle$ is governed by a nontrivial topological Hamiltonian $\hat{H}_{F1}$, fulfilling a quantum quench from $m_y \gg 1$ to $m_y = 0$. In this y-direction quench process, the BIS appears when $n_{1y} = 0$ [61], which yields $k_x^{\mathrm{BIS}} = 0, \pi$. After the quantum quench, we measure the time evolution of the spin polarization $\langle\hat{\sigma}_{x,y}\rangle$ for each k_x in the Brillouin zone, from which we extract the time-averaged spin polarization $\overline{\langle\hat{\sigma}_{x,y}\rangle} = \frac{1}{N}\sum_{t=1}^{N}\langle\hat{\sigma}_{x,y}\rangle_t$, with the time-resolved spin polarization $\langle\hat{\sigma}_{x,y}\rangle_t = \langle\psi(t=0)|(\hat{U}_1^{-1})^t \cdot \hat{\sigma}_{x,y}(\hat{U}_1)^t|\psi(t=0)\rangle$.

When N is very large, the BISs k_x^{BIS} and the topological winding number ν_1 both can be directly measured through $\overline{\langle\hat{\sigma}_{x,y}\rangle}$ [61]; i.e.,

$$\overline{\langle\hat{\sigma}_y(k_x^{\mathrm{BIS}})\rangle} = 0, \quad \nu_1 = \frac{1}{2}[g_x(k_x^{\mathrm{BIS}} = \pi) - g_x(k_x^{\mathrm{BIS}} = 0)], \tag{9}$$

where $g_x(k_x^{\mathrm{BIS}}) = -\mathrm{sgn}(\partial_{k_\perp}\overline{\langle\hat{\sigma}_x\rangle})$ is related to the sign of the slope of the time-averaged spin polarization $\overline{\langle\hat{\sigma}_x\rangle}$ at BISs, with $k_\perp$ denoting the momentum perpendicular to BIS and points from $n_{1y} < 0$ to $n_{1y} > 0$. The theoretical results for $N = 60$ are presented in Fig. 3(b), showing that $\overline{\langle\hat{\sigma}_y(k_x^{\mathrm{BIS}} = 0, \pi)\rangle} = 0$ and $g_x(k_x^{\mathrm{BIS}} = \pi) = -g_x(k_x^{\mathrm{BIS}} = 0) = 1$.

The achievable repetition number N is limited by the coherence time T_2^* of the electron spin [$T_2^* \approx 2.6$ μs measured with a Ramsey free precession sequence, as shown in Fig. 1(d)], which is also the main error source in the operation. We take the optimal number of $N = 10$, experimentally. Figure 3(a) shows the experimentally measured results of $\overline{\langle\hat{\sigma}_{x,y}\rangle}$ are in good agreement with the theoretical results. Based on these results, it is found that the time-averaged spin polarization $\overline{\langle\hat{\sigma}_y\rangle}$ is zero when $k_x = 0, \pi$, which allows us to clearly identify the BISs. Note that $n_{1y} > 0$ when $k_x \in (0, \pi)$; otherwise, $n_{1y} < 0$. Therefore, the slope of the time-averaged spin polarization $\overline{\langle\hat{\sigma}_x\rangle}$ at $k_x^{\mathrm{BIS}} = 0$ ($k_x^{\mathrm{BIS}} = \pi$) is recognized as 1 (−1), yielding $g_x(k_x^{\mathrm{BIS}} = \pi) = -g_x(k_x^{\mathrm{BIS}} = 0) = 1$. According to Eq. (9), we can determine the topological winding number value as $\nu_1 = 1$.

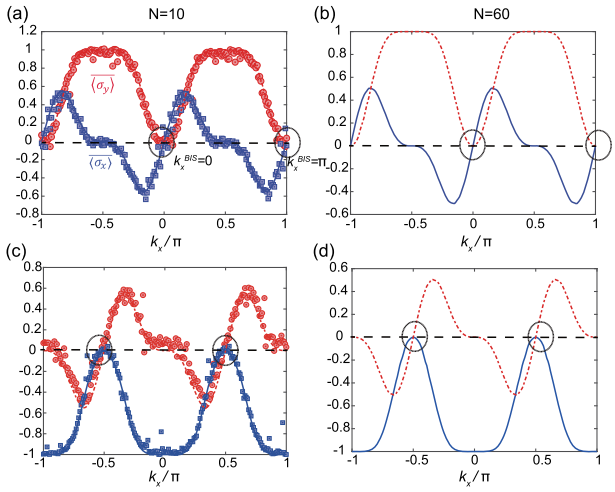

Fig. 3. Measurement of topological winding number (a) ν_1 and (c) ν_2 with $t_x = 0.5\pi$ and $t_y = 0.5\pi$. (a) The experimentally observed time-averaged spin polarizations $\overline{\langle\hat{\sigma}_{x,y}\rangle}$ as a function of k_x after $N = 10$ times $\hat{U}_1$. The associated theoretical result with repetition number $N = 60$ is plotted in (b). (c) The experimentally observed time-averaged spin polarizations $\overline{\langle\hat{\sigma}_{x,y}\rangle}$ as a function of k_x after $N = 10$ times $\hat{U}_2$. The associated theoretical results with repetition number $N = 60$ is plotted in (d). Red dash-dotted and blue solid lines represent the theoretical results of $\hat{\sigma}_y$ and $\hat{\sigma}_x$ while the red circles and blue squares show the experimental values of $\hat{\sigma}_y$ and $\hat{\sigma}_x$, respectively. Each data point has been averaged 5×10^6 repetitions.

To measure the topological winding number ν_2 in case (1), the initial state of the system is prepared into $|\psi(t=0)\rangle = (|g\rangle - |e\rangle)/\sqrt{2}$, the ground state of a trivial topological Hamiltonian $\hat{H}^i_{F2} = (m_x + n_{2x})\hat{\sigma}_x + n_{2y}\hat{\sigma}_y$ with $m_x \gg 1$. Subsequently, an x-direction quantum quench from $m_x \gg 1$ to $m_x = 0$ is implemented by repeating $\hat{U}_2$ N times, thus causing the time evolution of the initial state $|\psi(t=0)\rangle$ to be governed by a nontrivial topological Hamiltonian $\hat{H}_{F2}$. The BIS appears when $n_{2x} = 0$ [61], which gives $k_x^{\mathrm{BIS}} = \pm 0.5\pi$. The BISs and the topological winding number ν_2 are measured through [61]

$$\overline{\langle\hat{\sigma}_x(k_x^{\mathrm{BIS}})\rangle} = 0,$$
$$\nu_2 = \frac{1}{2}[g_y(k_x^{\mathrm{BIS}} = 0.5\pi) - g_y(k_x^{\mathrm{BIS}} = -0.5\pi)], \tag{10}$$

where $g_y(k_x^{\mathrm{BIS}}) = -\mathrm{sgn}(\partial_{k_\perp}\overline{\langle\hat{\sigma}_y\rangle})$ is related to the sign of the slope of the time-averaged spin polarization $\overline{\langle\hat{\sigma}_y\rangle}$ at the BISs, with $k_\perp$ denoting the momentum perpendicular to BIS and pointing from $n_{2x} < 0$ to $n_{2x} > 0$. As theoretically presented in Fig. 3(d) for $N = 60$, $\overline{\langle\hat{\sigma}_x(k_x^{\mathrm{BIS}} = 0, \pi)\rangle} = 0$ and $g_y(k_x^{\mathrm{BIS}} = 0.5\pi) = -g_y(k_x^{\mathrm{BIS}} = -0.5\pi) = 1$. The corresponding experimental results for $N = 10$ are shown in Fig. 3(c) and agree well with theoretical results. From these experimental results, we can unambiguously conclude $\overline{\langle\hat{\sigma}_x(k_x = \pm 0.5\pi)\rangle} = 0$ and $g_y(k_x^{\mathrm{BIS}} = 0.5\pi) = -g_y(k_x^{\mathrm{BIS}} = -0.5\pi) = 1$, identifying the location of the BISs and the value of the topological winding number $\nu_2 = 1$. Hence, according to Eq. (7), the 0- and π-energy topological invariants are measured as $\nu_0 = 1$ and $\nu_\pi = 0$.

Regarding case (2), the same procedure is applied to extract the topological winding number ν_1 and ν_2. The experimental results on the time-averaged spin polarizations after $N = 10$ times $\hat{U}_1$ and $\hat{U}_2$ are shown in Figs. 4(a) and 4(c), respectively, which agree well with the theoretical results. Figure 4(a) illustrates that the BIS appears at $k_x^{\mathrm{BIS}} = 0, \pi$ in which $\overline{\langle\sigma_y\rangle} = 0$ and $g_x(k_x^{\mathrm{BIS}} = \pi) = -g_x(k_x^{\mathrm{BIS}} = 0) = 1$. The value of the topological winding number is measured through $\nu_1 = \frac{1}{2}[g_x(k_x^{\mathrm{BIS}} = \pi) - g_x(k_x^{\mathrm{BIS}} = 0)] = 1$. Figure 4(c) shows that the BIS appears at $k_x^{\mathrm{BIS}} = \pm 0.5\pi, \pm\arccos(\pm 0.4), \pm\arccos(\pm 0.8)$. At such points, $\overline{\langle\hat{\sigma}_x\rangle}$ is not strictly zero but still maximal and approaching zero. As suggested by the theoretical results shown in Fig. 4(d) for $N = 60$, the slight difference from zero is a result of the fact that the number N we chose in the experiment is not large enough. This does not affect the measurement of the slopes of the time-averaged spin

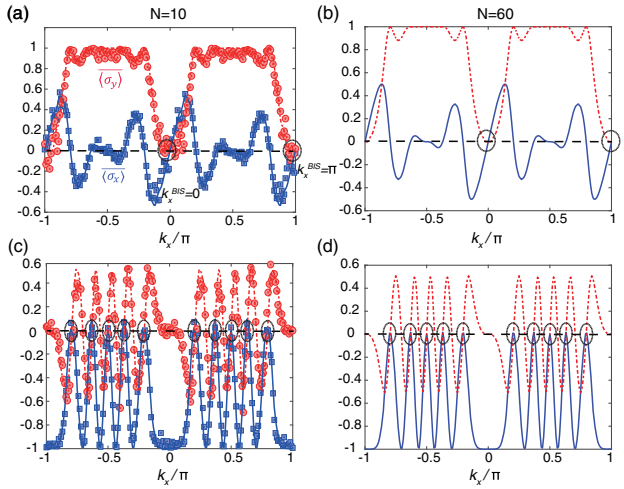

Fig. 4. Measurement of topological winding number (a) ν_1 and (c) ν_2 with $t_x = 2.5\pi$ and $t_y = 0.5\pi$. (a) The experimentally observed time-averaged spin polarizations $\overline{\langle\hat{\sigma}_{x,y}\rangle}$ as a function of k_x after $N = 10$ times $\hat{U}_1$. The associated theoretical result with repetition number $N = 60$ is plotted in (b). (c) The experimentally observed time-averaged spin polarizations $\overline{\langle\hat{\sigma}_{x,y}\rangle}$ as a function of k_x after $N = 10$ times $\hat{U}_2$. The associated theoretical result with repetition number $N = 60$ is plotted in (d). Red dash-dotted and blue solid lines represent theoretical results of $\hat{\sigma}_y$ and $\hat{\sigma}_x$ while the red circles and blue squares show the experimental values of $\hat{\sigma}_y$ and $\hat{\sigma}_x$, respectively. Each data point has been averaged 5×10^6 repetitions.

polarization $\overline{\langle\sigma_y\rangle}$ at the BISs; i.e., $g_y(k_x^{\mathrm{BIS}} \in k_+) = -g_y(k_x^{\mathrm{BIS}} \in k_-) = 1$, where $k_+ = 0.5\pi, \arccos(\pm 0.8), -\arccos(\pm 0.4)$ and $k_- = -0.5\pi, -\arccos(\pm 0.8), \arccos(\pm 0.4)$. The topological winding number ν_2 is measured through $\nu_2 = \frac{1}{2}[\sum_{k_x^{\mathrm{BIS}} \in k_+} g_y(k_x^{\mathrm{BIS}}) - \sum_{k_x^{\mathrm{BIS}} \in k_-} g_y(k_x^{\mathrm{BIS}})]$, giving the value of the topological winding number as $\nu_2 = 5$. Substituting the above values into Eq. (7), the 0- and π-energy topological invariants are determined as $\nu_0 = 3$ and $\nu_\pi = -2$.

We emphasize that $g_{x,y}(k_x^{\mathrm{BIS}})$ is related to the slopes of the time-averaged spin polarizations $\overline{\langle\sigma_{x,y}\rangle}$ at the BISs and quite robust to the experimental imperfections. This feature manifests topological protection and enables accurate measurements of the topological invariants of the Floquet topological phases.

3. DISCUSSION AND CONCLUSION

In summary, we have reported the digital simulation and detection of Floquet topological phases with a solid-state quantum simulator. To measure Floquet topological invariants, quantum quenches of Floquet topological phases are digitally simulated. The method developed here can be directly applied to other well-developed platforms of quantum simulators, such as superconducting circuits and trapped ions. We believe our work opens the door for the DQS of topological phases with programmable quantum simulators, including high-dimensional Floquet topological insulators [2–4,62], Floquet Z_2 topological phases [63], and Floquet Hopf insulators [64] that are hard to engineer in other topological systems. This also paves the way for DQS of nonequilibrium topological phases [65–67], where quantum quenches could be digitally simulated.

Funding. National Key Research and Development Program of China (2020YFA0309400, 2017YFA0304203, 2018YFA0306600, 2018YFF01012500); Newton Fund (NF170876); Fund for Shanxi 1331 Project Key Subjects Construction and 111 Project (D18001); PCSIRT (IRT-17R70); National Natural Science Foundation of China (11604069, 11904070, 12074234); Fundamental Research Funds for the Central Universities (PA2019GDQT0023); Program of State Key Laboratory of Quantum Optics and Quantum Optics Devices (KF201802).

Disclosures. The authors declare that there are no conflicts of interest related to this paper.

REFERENCES

1. R. Moessner and S. L. Sondhi, "Equilibration and order in quantum Floquet matter," Nat. Phys. **13**, 424–428 (2017).
2. T. Kitagawa, E. Berg, M. Rudner, and E. Demler, "Topological characterization of periodically driven quantum systems," Phys. Rev. B **82**, 235114 (2010).
3. M. S. Rudner, N. H. Lindner, E. Berg, and M. Levin, "Anomalous edge states and the bulk-edge correspondence for periodically driven two-dimensional systems," Phys. Rev. X **3**, 031005 (2013).
4. N. H. Lindner, G. Refael, and V. Galitski, "Floquet topological insulator in semiconductor quantum wells," Nat. Phys. **7**, 490–495 (2011).
5. L. Jiang, T. Kitagawa, J. Alicea, A. R. Akhmerov, D. Pekker, G. Refael, J. I. Cirac, E. Demler, M. D. Lukin, and P. Zoller, "Majorana fermions in equilibrium and in driven cold-atom quantum wires," Phys. Rev. Lett. **106**, 220402 (2011).
6. M. Thakurathi, A. A. Patel, D. Sen, and A. Dutta, "Floquet generation of Majorana end modes and topological invariants," Phys. Rev. B **88**, 155133 (2013).
7. A. Kundu and B. Seradjeh, "Transport signatures of Floquet Majorana fermions in driven topological superconductors," Phys. Rev. Lett. **111**, 136402 (2013).
8. J. K. Asbóth, B. Tarasinski, and P. Delplace, "Chiral symmetry and bulk-boundary correspondence in periodically driven one-dimensional systems," Phys. Rev. B **90**, 125143 (2014).
9. V. D. Lago, M. Atala, and L. E. F. Torres, "Floquet topological transitions in a driven one-dimensional topological insulator," Phys. Rev. A **92**, 023624 (2015).
10. M. Fruchart, "Complex classes of periodically driven topological lattice systems," Phys. Rev. B **93**, 115429 (2016).
11. S. Lloyd, "Universal quantum simulators," Science **273**, 1073–1078 (1996).
12. I. Buluta and F. Nori, "Quantum simulators," Science **326**, 108–111 (2009).
13. I. Bloch, J. Dalibard, and W. Zwerger, "Many-body physics with ultracold gases," Rev. Mod. Phys. **80**, 885 (2008).
14. M. Lewenstein, A. Sanpera, V. Ahufinger, B. Damski, A. Sen(De), and U. Sen, "Ultracold atomic gases in optical lattices: mimicking condensed matter physics and beyond," Adv. Phys. **56**, 243–379 (2007).
15. C. Gross and I. Bloch, "Quantum simulations with ultracold atoms in optical lattices," Science **357**, 995–1001 (2017).
16. R. Blatt and C. F. Roos, "Quantum simulations with trapped ions," Nat. Phys. **8**, 277–284 (2012).
17. K. Kim, M.-S. Chang, S. Korenblit, R. Islam, E. E. Edwards, J. K. Freericks, G.-D. Lin, L.-M. Duan, and C. Monroe, "Quantum simulation of frustrated Ising spins with trapped ions," Nature **465**, 590–593 (2010).
18. A. A. Houck, H. E. Türeci, and J. Koch, "On-chip quantum simulation with superconducting circuits," Nat. Phys. **8**, 292–299 (2012).
19. F. Arute, K. Arya, R. Babbush, D. Bacon, J. C. Bardin, R. Barends, R. Biswas, S. Boixo, F. G. S. L. Brandao, D. A. Buell, B. Burkett, Y. Chen, Z. Chen, B. Chiaro, R. Collins, W. Courtney, A. Dunsworth, E. Farhi, B. Foxen, A. Fowler, C. Gidney, M. Giustina, R. Graff, K. Guerin, S. Habegger, M. P. Harrigan, M. J. Hartmann, A. Ho, M. Hoffmann,

T. Huang, T. S. Humble, S. V. Isakov, E. Jeffrey, Z. Jiang, D. Kafri, K. Kechedzhi, J. Kelly, P. V. Klimov, S. Knysh, A. Korotkov, F. Kostritsa, D. Landhuis, M. Lindmark, E. Lucero, D. Lyakh, S. Mandrà, J. R. McClean, M. McEwen, A. Megrant, X. Mi, K. Michielsen, M. Mohseni, J. Mutus, O. Naaman, M. Neeley, C. Neill, M. Y. Niu, E. Ostby, A. Petukhov, J. C. Platt, C. Quintana, E. G. Rieffel, P. Roushan, N. C. Rubin, D. Sank, K. J. Satzinger, V. Smelyanskiy, K. J. Sung, M. D. Trevithick, A. Vainsencher, B. Villalonga, T. White, Z. J. Yao, P. Yeh, A. Zalcman, H. Neven, and J. M. Martinis, "Quantum supremacy using a programmable superconducting processor," Nature **574**, 505–510 (2019).

20. A. Aspuru-Guzik and P. Walther, "Photonic quantum simulators," Nat. Phys. **8**, 285–291 (2012).
21. N. Goldman, J. C. Budich, and P. Zoller, "Topological quantum matter with ultracold gases in optical lattices," Nat. Phys. **12**, 639–645 (2016).
22. D.-W. Zhang, Y.-Q. Zhu, Y. X. Zhao, H. Yan, and S.-L. Zhu, "Topological quantum matter with cold atoms," Adv. Phys. **67**, 253–402 (2019).
23. N. R. Cooper, J. Dalibard, and I. B. Spielman, "Topological bands for ultracold atoms," Rev. Mod. Phys. **91**, 015005 (2019).
24. F. Kong, C. Ju, Y. Liu, C. Lei, M. Wang, X. Kong, P. Wang, P. Huang, Z. Li, F. Shi, L. Jiang, and J. Du, "Direct measurement of topological numbers with spins in diamond," Phys. Rev. Lett. **117**, 060503 (2016).
25. W. Ma, L. Zhou, Q. Zhang, M. Li, C. Cheng, J. Geng, X. Rong, F. Shi, J. Gong, and J. Du, "Experimental observation of a generalized Thouless pump with a single spin," Phys. Rev. Lett. **120**, 120501 (2018).
26. W. Lian, S.-T. Wang, S. Lu, Y. Huang, F. Wang, X. Yuan, W. Zhang, X. Ouyang, X. Wang, X. Huang, L. He, X. Chang, D.-L. Deng, and L. Duan, "Machine learning topological phases with a solid-state quantum simulator," Phys. Rev. Lett. **122**, 210503 (2019).
27. J. S. Xu, K. Sun, Y. J. Han, C. F. Li, J. K. Pachos, and G. C. Guo, "Simulating the exchange of Majorana zero modes with a photonic system," Nat. Commun. **7**, 13194 (2016).
28. Y. Wang, Y. H. Lu, F. Mei, J. Gao, Z. M. Li, H. Tang, S. L. Zhu, S. Jia, and X. M. Jin, "Direct observation of topology from single-photon dynamics on a photonic chip," Phys. Rev. Lett. **122**, 193903 (2019).
29. J. S. Xu, K. Sun, J. K. Pachos, Y. J. Han, C. F. Li, and G. C. Guo, "Photonic implementation of Majorana-based Berry phases," Sci. Adv. **4**, eaat6533 (2018).
30. W. Cai, J. Han, F. Mei, Y. Xu, Y. Ma, X. Li, H. Wang, Y. P. Song, Z.-Y. Xue, Z.-Q. Yin, S. Jia, and L. Sun, "Observation of topological magnon insulator states in a superconducting circuit," Phys. Rev. Lett. **123**, 080501 (2019).
31. A. D. King, J. Carrasquilla, J. Raymond, I. Ozfidan, E. Andriyash, A. Berkley, M. Reis, T. Lanting, R. Harris, F. Altomare, K. Boothby, P. I. Bunyk, C. Enderud, A. Fréchette, E. Hoskinson, N. Ladizinsky, T. Oh, G. Poulin-Lamarre, C. Rich, Y. Sato, A. Y. Smirnov, L. J. Swenson, M. H. Volkmann, J. Whittaker, J. Yao, E. Ladizinsky, M. W. Johnson, J. Hilton, and M. H. Amin, "Observation of topological phenomena in a programmable lattice of 1,800 qubits," Nature **560**, 456–460 (2018).
32. E. Flurin, V. V. Ramasesh, S. Hacohen-Gourgy, L. S. Martin, N. Y. Yao, and I. Siddiqi, "Observing topological invariants using quantum walks in superconducting circuits," Phys. Rev. X **7**, 031023 (2017).
33. M. D. Schroer, M. H. Kolodrubetz, W. F. Kindel, M. Sandberg, J. Gao, M. R. Vissers, D. P. Pappas, A. Polkovnikov, and K. W. Lehnert, "Measuring a topological transition in an artificial spin-1/2 system," Phys. Rev. Lett. **113**, 050402 (2014).
34. P. Roushan, C. Neill, Y. Chen, M. Kolodrubetz, C. Quintana, N. Leung, M. Fang, R. Barends, B. Campbell, Z. Chen, B. Chiaro, A. Dunsworth, E. Jeffrey, J. Kelly, A. Megrant, J. Mutus, P. J. J. O'Malley, D. Sank, A. Vainsencher, J. Wenner, T. White, A. Polkovnikov, A. N. Cleland, and J. M. Martinis, "Observation of topological transitions in interacting quantum circuits," Nature **515**, 241–244 (2014).
35. Y. P. Zhong, D. Xu, P. Wang, C. Song, Q. J. Guo, W. X. Liu, K. Xu, B. X. Xia, C.-Y. Lu, S. Han, J.-W. Pan, and H. Wang, "Emulating anyonic fractional statistical behavior in a superconducting quantum circuit," Phys. Rev. Lett. **117**, 110501 (2016).
36. T. Wang, Z. Zhang, L. Xiang, Z. Gong, J. Wu, and Y. Yin, "Simulating a topological transition in a superconducting phase qubit by fast adiabatic trajectories," Sci. China Phys. Mech. Astron. **61**, 047411 (2018).
37. X. Tan, D.-W. Zhang, Q. Liu, G. Xue, H.-F. Yu, Y.-Q. Zhu, H. Yan, S.-L. Zhu, and Y. Yu, "Topological Maxwell metal bands in a superconducting qutrit," Phys. Rev. Lett. **120**, 130503 (2018).
38. C. Song, D. Xu, P. Zhang, J. Wang, Q. Guo, W. Liu, K. Xu, H. Deng, K. Huang, D. Zheng, S.-B. Zheng, H. Wang, X. Zhu, C.-Y. Lu, and J.-W. Pan, "Demonstration of topological robustness of anyonic braiding statistics with a superconducting quantum circuit," Phys. Rev. Lett. **121**, 030502 (2018).
39. X. Tan, Y. X. Zhao, Q. Liu, G. Xue, H. F. Yu, Z. D. Wang, and Y. Yu, "Simulation and manipulation of tunable Weyl-semimetal bands using superconducting quantum circuits," Phys. Rev. Lett. **122**, 010501 (2019).
40. B. P. Lanyon, C. Hempel, D. Nigg, M. Müller, R. Gerritsma, F. Zähringer, P. Schindler, J. T. Barreiro, M. Rambach, G. Kirchmair, M. Hennrich, P. Zoller, R. Blatt, and C. F. Roos, "Universal digital quantum simulation with trapped ions," Science **334**, 57–61 (2011).
41. M. Müller, S. Diehla, G. Pupillo, and P. Zoller, "Engineered open systems and quantum simulations with atoms and ions," Adv. Atom. Mol. Opt. Phys. **61**, 1–80 (2012).
42. I. M. Georgescu, S. Ashhab, and F. Nori, "Quantum simulation," Rev. Mod. Phys. **86**, 153–185 (2014).
43. L. Lamata, A. Parra-Rodriguez, M. Sanz, and E. Solano, "Digital-analog quantum simulations with superconducting circuits," Adv. Phys. X **3**, 1457981 (2018).
44. H. Weimer, M. Müller, I. Lesanovsky, P. Zoller, and H. P. Büchler, "A Rydberg quantum simulator," Nat. Phys. **6**, 382–388 (2010).
45. A. Mezzacapo, J. Casanova, L. Lamata, and E. Solano, "Digital quantum simulation of the Holstein model in trapped ions," Phys. Rev. Lett. **109**, 200501 (2012).
46. J. Casanova, A. Mezzacapo, L. Lamata, and E. Solano, "Quantum simulation of interacting fermion lattice models in trapped ions," Phys. Rev. Lett. **108**, 190502 (2012).
47. U. L. Heras, A. Mezzacapo, L. Lamata, S. Filipp, A. Wallraff, and E. Solano, "Digital quantum simulation of spin systems in superconducting circuits," Phys. Rev. Lett. **112**, 200501 (2014).
48. R. Barends, L. Lamata, J. Kelly, L. García-Álvarez, A. G. Fowler, A. Megrant, E. Jeffrey, T. C. White, D. Sank, J. Y. Mutus, B. Campbell, Y. Chen, Z. Chen, B. Chiaro, A. Dunsworth, I.-C. Hoi, C. Neill, P. J. J. O'Malley, C. Quintana, P. Roushan, A. Vainsencher, J. Wenner, E. Solano, and J. M. Martinis, "Digital quantum simulation of fermionic models with a superconducting circuit," Nat. Commun. **6**, 7654 (2015).
49. Y. Salathé, M. Mondal, M. Oppliger, J. Heinsoo, P. Kurpiers, A. Potočnik, A. Mezzacapo, U. Las Heras, L. Lamata, E. Solano, S. Filipp, and A. Wallraff, "Digital quantum simulation of spin models with circuit quantum electrodynamics," Phys. Rev. X **5**, 021027 (2015).
50. R. Barends, A. Shabani, L. Lamata, J. Kelly, A. Mezzacapo, U. L. Heras, R. Babbush, A. G. Fowler, B. Campbell, Y. Chen, Z. Chen, B. Chiaro, A. Dunsworth, E. Jeffrey, E. Lucero, A. Megrant, J. Y. Mutus, M. Neeley, C. Neill, P. J. J. O'Malley, C. Quintana, P. Roushan, D. Sank, A. Vainsencher, J. Wenner, T. C. White, E. Solano, H. Neven, and J. M. Martinis, "Digitized adiabatic quantum computing with a superconducting circuit," Nature **534**, 222–226 (2016).
51. C. Ju, C. Lei, X. Xu, D. Culcer, Z. Zhang, and J. Du, "NV-center-based digital quantum simulation of a quantum phase transition in topological insulators," Phys. Rev. B **89**, 045432 (2014).
52. T. van der Sar, Z. H. Wang, M. S. Blok, H. Bernien, T. H. Taminiau, D. M. Toyli, D. A. Lidar, D. D. Awschalom, R. Hanson, and V. V. Dobrovitski, "Decoherence-protected quantum gates for a hybrid solid-state spin register," Nature **484**, 82–86 (2012).
53. Y. Wu, Y. Wang, X. Qin, X. Rong, and J. Du, "A programmable two-qubit solid-state quantum processor under ambient conditions," npj Quantum Inf. **5**, 9 (2019).
54. Q. Cheng, Y. Pan, H. Wang, C. Zhang, D. Yu, A. Gover, H. Zhang, T. Li, L. Zhou, and S. Zhu, "Observation of anomalous π modes in photonic Floquet engineering," Phys. Rev. Lett. **122**, 173901 (2019).
55. A. Stern and N. H. Lindner, "Topological quantum computation-from basic concepts to first experiments," Science **339**, 1179–1184 (2013).
56. C. Nayak, S. H. Simon, A. Stern, M. Freedman, and S. D. Sarma, "Non-Abelian anyons and topological quantum computation," Rev. Mod. Phys. **80**, 1083 (2008).

57. L. Zhou and J. Gong, "Floquet topological phases in a spin-1/2 double kicked rotor," Phys. Rev. A **97**, 063603 (2018).
58. L. Zhou and J. Gong, "Non-Hermitian Floquet topological phases with arbitrarily many real-quasienergy edge states," Phys. Rev. B **98**, 205417 (2018).
59. $n_{1x} = \sin[t_x \cos(k_x)) \cos(t_y \sin(k_x)]$, $n_{1y} = \sin[t_y \sin(k_x)]$, $n_{2x} = \sin[t_x \cos(k_x)]$, $n_{2y} = \cos[t_x \cos(k_x)] \sin[t_y \sin(k_x)]$.
60. B. Chen, J. Geng, F. Zhou, L. Song, H. Shen, and N. Xu, "Quantum state tomography of a single electron spin in diamond with Wigner function reconstruction," Appl. Phys. Lett. **114**, 041102 (2019).
61. L. Zhang, L. Zhang, S. Niu, and X.-J. Liu, "Dynamical classification of topological quantum phases," Sci. Bull. **63**, 1385–1391 (2018).
62. N. H. Lindner, D. L. Bergman, G. Refael, and V. Galitski, "Topological Floquet spectrum in three dimensions via a two-photon resonance," Phys. Rev. B **87**, 235131 (2013).
63. D. Carpentier, P. Delplace, M. Fruchart, and K. Gawedzki, "Topological index for periodically driven time-reversal invariant 2D systems," Phys. Rev. Lett. **114**, 106806 (2015).
64. T. Schuster, S. Gazit, J. E. Moore, and N. Y. Yao, "Floquet Hopf insulators," Phys. Rev. Lett. **123**, 266803 (2019).
65. Y. Hu, P. Zoller, and J. C. Budich, "Dynamical buildup of a quantized Hall response from nontopological states," Phys. Rev. Lett. **117**, 126803 (2016).
66. J. H. Wilson, J. C. W. Song, and G. Refael, "Remnant geometric Hall response in a quantum quench," Phys. Rev. Lett. **117**, 235302 (2016).
67. F. N. Unal, E. J. Mueller, and M. O. Oktel, "Nonequilibrium fractional Hall response after a topological quench," Phys. Rev. A **94**, 053604 (2016).